AIAA 80-0278R

Alternative to the e^9 Procedure for Predicting Boundary-Layer Transition

D. C. Wilcox*
DCW Industries, Inc., Studio City, Calif.

A method has been devised that can be used in conjunction with linear-stability theory for predicting boundary-layer transition. As with the classical "e^9" procedure, for a given frequency the growth of a disturbance is computed downstream of the initial point of instability using the linearized equations of motion. In contrast to the e^9 procedure in which the linearized equations are used all the way to the inferred transition point, an approximate set of long-time averaged equations that account for nonlinearity is used to describe the ultimate nonlinear growth of the disturbance. Because the new method accounts for nonlinear processes it holds promise as a more physically sound procedure than the e^9 method for determining the point at which a boundary layer undergoes transition to turbulence.

I. Introduction

ADVANCED design of aerodynamic and hydrodynamic vehicles often depends critically upon an understanding of transition sensitivity to many phenomena. Nosetips on ballistic re-entry vehicles, for example, must be designed to withstand transition destabilizing effects of surface roughness, ablation, surface cooling (in the presence of roughness), and entropy gradient. As a second example, current advanced hydrodynamic vehicle design procedures make advantageous use of the strong stabilizing effects of favorable pressure gradient and surface heating to generate laminar-flow vehicles. Linear stability theory is the most popular theoretical tool for guiding design on many vehicles for which transition location influences the design configuration. While linear stability theory has limited utility for re-entry vehicle nosetips (because of the occurrence of roughness-induced transition bypass), a great deal of success with stability theory has been enjoyed for hydrodynamic vehicles, most notably by Wazzan and Smith.[1]

For transition triggered by small amplitude disturbances, linear-stability theory provides a nearly exact solution to the Navier-Stokes equations. There is little doubt that stability theory's Tollmien-Schlichting waves exist and play an important role in the initial stages of transition. Because the end state of the transition process is a (highly nonlinear) turbulent flow, linear stability theory breaks down at some point between that of the initiation of Tollmien-Schlichting waves and the transition point (defined, for example, as the point where skin friction achieves a minimum). In other words, linear stability theory is inapplicable in the postcritical stages of transition and therefore has no natural way of specifying the actual transition point.

Undaunted by this limitation on stability theory's applicability, Smith[2] and van Ingen[3] simultaneously (with no knowledge of the other's activities) devised the well-known e^9 method. As is so often the case with clever approximations, the e^9 method has yielded accurate predictions for flows well beyond the original data base. However, the record of success has been blemished somewhat by inaccurate predictions.

Presumably, either a nonlinear stability theory or an exact Navier-Stokes solution method is needed to rigorously bridge the gap between the initiation of Tollmien-Schlichting waves and the transition point. Because neither of these two approaches has been developed to the point of being practicable for engineering design, the designer must depend upon existing correlations and/or approximate methods such as the e^9 method. While such methods have yielded some useful information, generally speaking, reliable quantitative predictions can be made only for the simplest of flows. This is a quite unsatisfactory state of affairs as advanced vehicles invariably involve subtle geometries and other complicating effects. Clearly, new prediction methods are needed.

Recently, a new approximate transition-prediction method has been devised that shows great promise for engineering design, viz., the turbulence-model transition-prediction method.[4-6] The method is based on the conventional long-time averaged equations of motion. Nonlinear correlation terms such as the Reynolds stress are approximated in a manner similar to that used in standard closure schemes for turbulent flow modeling. Turbulence-model equations on the one hand are expected to apply in the latter stages of transition. On the other hand, the time-averaging process removes explicit appearance of Tollmien-Schlichting waves. Consequently, the turbulence-model transition-prediction method is reasonably well founded only near the end of transition.

As with the linear-stability/e^9 method, turbulence-model equations have provided accurate transition predictions well beyond the original data base. In fact, the equations formulated by Wilcox and Chambers[7-11] have yielded accurate results for virtually all of the applications made to date. However, some of this success has been achieved with an adjustable parameter, viz., the freestream turbulence level. Additionally, the method has no natural way of representing spectral effects.

In summary, because correlations generally are limited to a restricted data base, linear-stability/e^9 and turbulence-model methods are the only two comprehensive transition theories that are of practical utility for the aerodynamic/hydrodynamic vehicle designer. The former is theoretically sound only during the initial stages of transition while the latter is well founded only near the end of transition. Hence, we reasonably may speculate that a synthesis of these two methods will yield a transition-prediction theory that is fundamentally more sound than either theory standing alone.

The primary objective of this research study has been to synthesize linear-stability theory and the turbulence-model transition-prediction method. In so doing, the most immediate result of the proposed research, if successful, would be development of a physically sound alternative to the empirical Smith-van Ingen e^9 procedure. Aside from the advantage of having a more fundamental method for simulating the postcritical stages of transition, the proposed

Presented as Paper 80-0278 at the AIAA 18th Aerospace Sciences Meeting, Pasadena, Calif., Jan. 14-16, 1980; submitted Jan. 16, 1980; revision received July 3, 1980. Copyright © American Institute of Aeronautics and Astronautics, Inc., 1980. All rights reserved.

*President. Associate Fellow AIAA.

synthesis would obviate the costly eigensolutions needed to compute amplification ratios beyond the critical Reynolds number. Rather, a straightforward boundary-layer marching computation would be all that is needed in solving the turbulence/transition model equations from the critical Reynolds number up to the transition Reynolds number.

As will be shown in the following sections, an important first step has been taken toward accomplishing the proposed synthesis. Results for boundary layers with and without pressure gradient show that the most important (in the context of transitional boundary layers) closure coefficient appearing in the turbulence-model equations approaches a universal limiting value for amplification ratios in excess of about e^4. Using this limiting value, accurate transition predictions have been made for the Blasius boundary layer.

Section II reviews the basic formulation underlying our theoretical approach. In Sec. III, the Blasius boundary layer is analyzed including comparison of predicted and experimentally-measured transition points. Effects of both adverse and favorable pressure gradient are addressed in Sec. IV. Results and conclusions follow in Sec. V.

II. Theoretical Formulation

In this section, for the sake of completeness, we first review the overall approach. Then the turbulence model equations underlying the approach are presented. Finally, the manner in which turbulence-model parameters are computed from a given linear-stability solution is delineated.

A. Overview

Conceptually, our overall approach to predicting boundary-layer transition consists of three inter-related phases. In the first phase conventional linear-stability computations are performed up to and beyond the point at which a disturbance becomes unstable. As a key feature of these first-phase computations we have found empirically that the computations are most appropriately terminated when the initial disturbance has been amplified by a factor of e^4. In the second phase the linear-stability solutions at the e^4-amplification point are used to compute key turbulence model parameters which are needed to specify a key closure coefficient as well as initial and boundary conditions for a subsequent turbulence-model calculation. In the third phase a boundary-layer program incorporating the Wilcox-Traci[10-11] turbulence-model equations is used to predict the actual transition point. Most notably, a range of frequencies is considered in all phases of the computational procedure.

The rationale of this approach is twofold. First, using linear-stability theory in the initial phase of the procedure allows us to take proper account of the transition phenomenon's sensitivity to the frequency of the disturbance. Using the turbulence-model equations is quite inappropriate in the initial phase as long-time averaging (which is an integral aspect of the turbulence-model theory) precludes explicit representation of frequency effects. Second, using the turbulence-model equations in the final phase allows us (at least on a conceptual level) to represent nonlinear processes which ultimately must become dominant as the boundary layer nears transition to a turbulent state. Using linear-stability theory is quite inappropriate in the final phase as the linearization precludes explicit representation of nonlinear effects.

The astute reader will notice that a key premise is implicit in the rationale of our approach. Specifically, for this approach to work, it must be the case that either 1) the transition phenomenon is frequency independent beyond the e^4-amplification point or 2) a method exists whereby frequency effects can be explicitly expressed in the turbulence-model equations during the latter phases of transition. As will be demonstrated in this paper, while the transition process is somewhat frequency dependent beyond the e^4-amplification point, this frequency dependence can indeed be explicitly expressed in the model equations.

B. Turbulence-Model Equations

The two-equation model of turbulence developed by Wilcox and Traci[10-11] is used in this study for predicting boundary-layer development during the latter phases of transition. For incompressible boundary layers this model consists of the long time averaged conservation of mass and momentum equations and two additional rate equations. Denoting arc length and surface-normal distance by x and y with corresponding velocity components u and v, the four equations of motion for incompressible boundary layers are:

$$\frac{\partial u}{\partial x}+\frac{\partial v}{\partial y}=0 \tag{1}$$

$$u\frac{\partial u}{\partial x}+v\frac{\partial u}{\partial y}=-\frac{dp}{dx}+\frac{\partial}{\partial y}\left\{(\nu+\epsilon)\frac{\partial u}{\partial y}\right\} \tag{2}$$

$$u\frac{\partial e}{\partial x}+v\frac{\partial e}{\partial y}=\left\{\alpha^*\left|\frac{\partial u}{\partial y}\right|-\beta^*\omega\right\}e+\frac{\partial}{\partial y}\left\{(\nu+\sigma^*\epsilon)\frac{\partial e}{\partial y}\right\} \tag{3}$$

$$u\frac{\partial \omega^2}{\partial x}+v\frac{\partial \omega^2}{\partial y}=\left\{\alpha\left|\frac{\partial u}{\partial y}\right|-\left[\beta+2\sigma\left(\frac{\partial \ell}{\partial y}\right)^2\right]\omega\right\}\omega^2 + \frac{\partial}{\partial y}\left\{(\nu+\sigma\epsilon)\frac{\partial \omega^2}{\partial y}\right\} \tag{4}$$

where p is pressure and ν is kinematic viscosity. The quantity ϵ is kinematic eddy viscosity which is computed as the ratio of specific turbulent mixing energy e to turbulent dissipation rate ω, i.e.,

$$\epsilon=e/\omega \tag{5}$$

Also, ℓ is the turbulence length scale computed according to

$$\ell=e^{1/2}/\omega \tag{6}$$

Finally, the quantities $\alpha,\alpha^*,\beta,\beta^*,\sigma$, and σ^* are closure coefficients whose values appropriate for turbulent flows have been found empirically[10] to be given by the following:

$$\beta=3/20,\ \beta^*=9/100\quad \sigma=1/2,\ \sigma^*=1/2$$

$$\alpha=(1/3)\{1-(1-\lambda)\exp(-Re_T/2)\}$$

$$\alpha^*=(3/10)\{1-(1-\lambda)\exp(-2Re_T)\} \tag{7}$$

where Re_T is Reynolds number based on turbulence properties defined as

$$Re_T=e^{1/2}\ell/\nu \tag{8}$$

and the quantity λ is an additional closure coefficient whose value has been found by Wilcox[11] to vary with freestream turbulence level, surface temperature, and pressure gradient. For the Blasius boundary layer a value of $\lambda=1/11$ has been found to yield transition-point predictions in reasonably close agreement with experimentally measured transition points.[10,11] Experience with the model equations[11] has shown that the model's ability to predict transition hinges most heavily upon the closure coefficient λ.

Equations (1-4) must be solved subject to boundary conditions at the surface, $y=0$, and at the boundary-layer edge, $y=\delta$, where δ is boundary-layer thickness. Prior studies have established that for perfectly-smooth surfaces (rough surfaces are not considered in this study), we must require

$$u=v=e=0 \text{ at } y=0 \tag{9}$$

and

$$\omega \to (20/\beta)(\nu/y^2) \quad \text{as} \quad y \to 0 \tag{10}$$

Denoting conditions at the boundary-layer edge by subscript e, we must also require

$$u = U_e(x) \quad \text{at} \quad y = \delta \tag{11}$$

while $e_e(x)$ and $\omega_e(x)$ must satisfy the following simplified equations:

$$U_e \frac{de_e}{dx} = -\beta^* \omega_e e_e \quad U_e \frac{d\omega_e^2}{dx} = -\beta \omega_e^3 \quad \text{at} \quad y = \delta \tag{12}$$

C. Computing Turbulence-Model Parameters from a Linear-Stability Solution

As stated in Subsec. A, before the turbulence-model phase of the computation can be initiated, initial and boundary conditions as well as the closure coefficient λ must be deduced from the linear-stability solution. To do so we must first note several important facts about the various turbulence-model parameters.

First of all, in order to define initial and boundary values for e and ω we note that Wilcox and Chambers[12] have defined these quantities in terms of the fluctuating vertical velocity v' according to the following:

$$e = (9/4)\langle v'^2 \rangle \tag{13}$$

and

$$\omega = \frac{3\nu}{\beta^*} \frac{\langle (\partial v'/\partial y)^2 \rangle}{\langle v'^2 \rangle} \tag{14}$$

where $\langle\ \rangle$ denotes long time average. As the linear-stability solution yields the instantaneous v' profile, Eqs. (13) and (14) are sufficient to determine e and ω profiles provided a suitable time-averaging process can be defined.

Next, in order to determine λ, we first rewrite Eq. (3) under the standard parallel-flow assumption (i.e., $v \equiv 0$) and in the limit of small turbulent Reynolds number (i.e., $Re_T \ll 1$). The result is

$$u \frac{\partial e}{\partial x} = \frac{3}{10} \lambda \left| \frac{\partial u}{\partial y} \right| e - \beta^* \omega e + \nu \frac{\partial^2 e}{\partial y^2} \tag{15}$$

Note that in the actual turbulence-model phase of the computation, Eq. (3) is used. Equation (15) has been introduced only to devise a method for computing λ from the linear-stability solution.

Now, noting the definition of e given in Eq. (13), we can derive an exact equation for its evolution by taking the v' moment of the v-momentum equation and time averaging. Assuming that in the limit $Re_T \to 0$ the triple correlation term is negligibly small and retaining parallel-flow and boundary-layer approximations, we obtain

$$u \frac{\partial e}{\partial x} = -\frac{9}{2} \left\langle \frac{v'}{\rho} \frac{\partial p'}{\partial y} \right\rangle - \frac{9}{2} \nu \left\langle \left(\frac{\partial v'}{\partial y} \right)^2 \right\rangle + \nu \frac{\partial^2 e}{\partial y^2} \tag{16}$$

Comparison of Eqs. (15) and (16) yields a procedure for defining λ in terms of the fluctuating quantities. Equating the net production (production less dissipation) terms shows that λ can be defined as follows:

$$\lambda = \frac{10}{3} \left[\nu \left\langle \left(\frac{\partial v'}{\partial y} \right)^2 \right\rangle - 2 \left\langle \frac{v'}{\rho} \frac{\partial p'}{\partial y} \right\rangle \right] \Big/ \langle v'^2 \rangle \left| \frac{\partial u}{\partial y} \right| \tag{17}$$

The final step in relating the linear stability and the turbulence-model parameters is to define an appropriate long-time average. To do so we note first that in the linear-stability solution the velocity and pressure fluctuations v' and p' are written as

$$v'(x,y,z,t) = U_\infty \phi(y) \exp\{i(\hat{\alpha}x + \hat{\beta}z - \hat{\omega}t)\} \tag{18}$$

$$p'(x,y,z,t) = \rho U_\infty^2 \pi(y) \exp\{i(\hat{\alpha}x + \hat{\beta}z - \hat{\omega}t)\} \tag{19}$$

where t denotes time, z is distance normal to the x and y axes, U_∞ is freestream velocity, ρ is density, $\hat{\alpha}$ and $\hat{\beta}$ are wave numbers, $\hat{\omega}$ is frequency, and the functions $\phi(y)$ and $\pi(y)$ are the complex amplitude functions of the fluctuating flow variables v' and p'.

To evaluate the time-averaged quantities appearing in Eqs. (13), (14), and (17) we use the following definition:

$$\langle \psi \rangle = \lim_{\hat{\omega}T \to \infty} \frac{1}{2T} \int_{t-T}^{t+T} \psi(x,y,z,\tau)\, d\tau \tag{20}$$

Then, working with the real parts of the linear-stability solution, performing all time averages indicated in Eqs. (13), (14), and (17), and denoting local Reynolds number by R yields the following:

$$e/U_\infty^2 = (9/8)(\phi_r^2 + \phi_i^2) \tag{21}$$

$$\frac{\nu\omega}{U_\infty^2} = \frac{3}{\beta^* R^2} \left[\left(\frac{d\phi_r}{d\eta} \right)^2 + \left(\frac{d\phi_i}{d\eta} \right)^2 \right] \Big/ (\phi_r^2 + \phi_i^2) \tag{22}$$

$$\lambda = \left[\left(\frac{d\phi_r}{d\eta} \right)^2 + \left(\frac{d\phi_i}{d\eta} \right)^2 - 2 \left(\phi_r \frac{d\pi_r}{d\eta} + \phi_i \frac{d\pi_i}{d\eta} \right) \right] \Big/ 0.3R(\phi_r^2 + \phi_i^2) \left| \frac{\partial U}{\partial \eta} \right| \tag{23}$$

where $U \equiv u/U_\infty$, subscripts r and i denote real and imaginary parts, and η is dimensionless distance defined by

$$\eta \equiv y\sqrt{U_e/\nu x} \tag{24}$$

with U_e denoting horizontal velocity at the boundary-layer edge. Note that for the constant-pressure case, $U_e = U_\infty$. Equations (21-23) are the desired relations which can be used to define λ and the initial and boundary conditions for a turbulence-model computation in terms of a given linear-stability solution.

III. Results for Constant Pressure

In this section we implement the basic method for the constant-pressure case, i.e., for the Blasius boundary layer. First, we compute the closure coefficient λ for a range of frequencies and demonstrate that beyond the e^4-amplification point λ asymptotes to a nearly frequency-independent profile. Next, we compute e and ω profiles at the e^4-amplification point which can be used to initiate a turbulence-model computation. Then, we establish boundary conditions for the turbulence-model phase. Finally, transition predictions are made and compared with experimental data.

A. Evaluation of the Closure Coefficient

A large number of linear-stability computations have been performed with the Mack[13] stability program; all computations have been done with the spatial amplification theory option. Both Reynolds number and frequency have been varied in order to determine the variation of λ throughout the Reynolds-number/frequency plane using Eq. (17).

Figure 1 shows computed λ profiles at nine Reynolds numbers corresponding to one stable case, a neutrally-stable case, and seven unstable cases corresponding to amplification from the neutral case by factors of e^n with values of n ranging

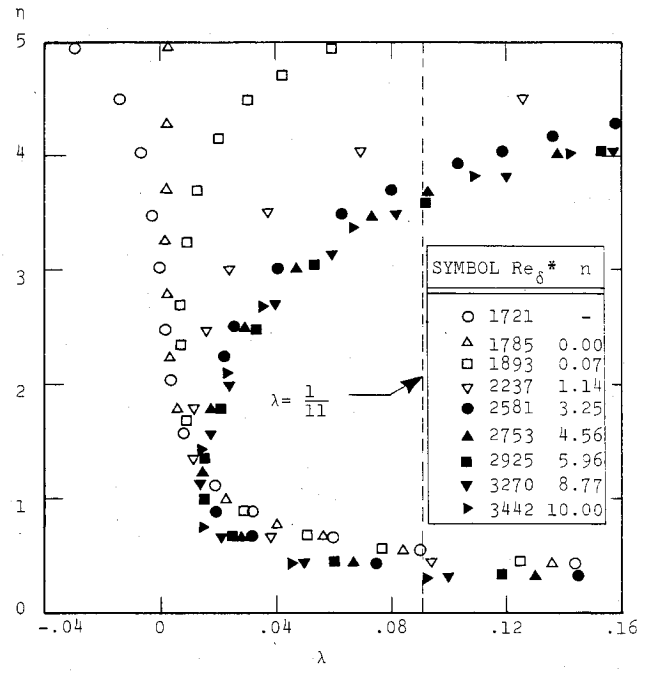

Fig. 1 Computed λ profiles for dimensionless frequency $Fr = 2 \times 10^{-5}$; zero pressure gradient.

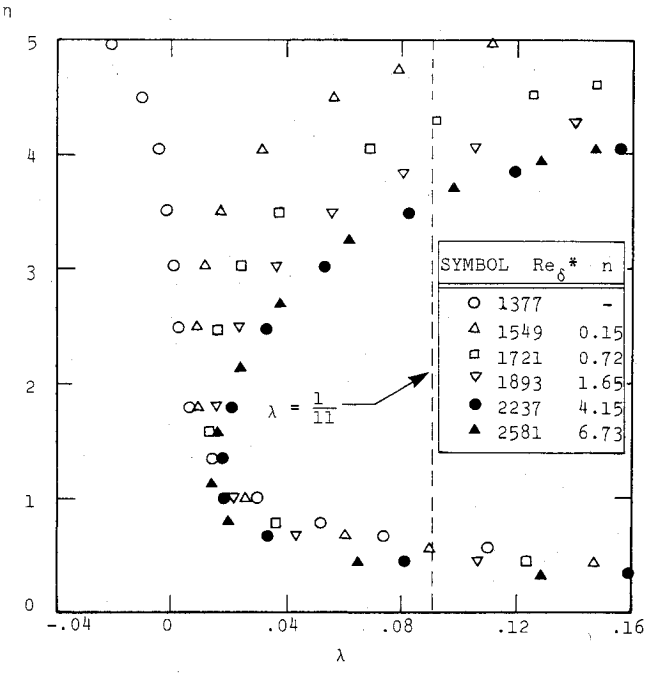

Fig. 2 Computed λ profiles for dimensionless frequency $Fr = 3 \times 10^{-5}$; zero pressure gradient.

0-10; for all nine cases the frequency is given by

$$Fr = \hat{\omega}\nu / U_\infty^2 = 2 \cdot 10^{-5} \tag{25}$$

We are thus following the evolution of λ for a constant-frequency disturbance at a Reynolds number upstream of the neutral point corresponding to the frequency given in Eq. (25).

As shown, although λ varies rapidly with y near the surface, all nine curves display approximately the same variation. However, above a value of $\eta = 2$, the various λ profiles vary rapidly with η and do so in dissimilar manner for amplification rates up to $e^{4.56}$. For example, at the lowest Reynolds number, for which the solution is stable, λ is negative above $\eta = 2$. As we move to the neutral point we find that λ vanishes for values of η in excess of 2.5. Then as Reynolds number increases, λ varies more and more rapidly with η and asymptotes to a single curve for amplification ratios in excess of between e^3 and e^4.

Figure 2 shows similar curves for a dimensionless frequency Fr given by

$$Fr = 3 \cdot 10^{-5} \tag{26}$$

Again, the curves collapse to a single curve for amplification ratios in excess of e^4.

Computations have been performed for frequencies covering the entire stability diagram. For each frequency considered the computed λ profiles always asymptote to a universal profile beyond the e^4-amplification point with a qualification. That is, as Reynolds number increases the upper branch of the stability diagram eventually is reached and we again enter a stable region. As we approach this upper neutral point, the λ profiles begin to fall back to those typical of low Reynolds numbers.

The rapid variation of λ near $\eta = 0$ results from a breakdown in the basic closure approximations near the surface. That is, the production term in the $\langle v'^2 \rangle$ equation, $\langle -v'/\rho \cdot \partial p'/\partial y \rangle$, goes to zero quadratically with distance from the surface so that, in terms of η,

$$\langle -v'/\rho \cdot \partial p'/\partial y \rangle \sim \eta^2 \quad \text{as} \quad \eta \to 0 \tag{27}$$

By contrast, the modeled production term for $Re_T \to 0$ behaves as

$$\frac{3}{10} \lambda \frac{\partial u}{\partial y} e \sim \lambda \eta^4 \qquad \text{as} \quad \eta \to 0 \tag{28}$$

Consequently, close to the surface we have

$$\lambda \sim \eta^{-2} \qquad \text{as} \quad \eta \to 0 \tag{29}$$

This modeling shortcoming is of little consequence as dissipation exceeds production near $\eta = 0$. Hence, for the remainder of this discussion our focus will be upon the region between $\eta = 1$ and the outer edge of the boundary layer, $\eta = 5$.

Figure 3 shows computed λ profiles for several frequencies and amplification ratios. As shown, all of the computed λ profiles cluster about the approximate profile defined by

$$\lambda = 0.0093 + 0.00156 \exp\{(10/7)(\eta - 1)\} \tag{30}$$

The fact that the computed λ profiles correlate with the profile defined in Eq. (30) independent of frequency is extremely important. This is our first indication that using the turbulence-model equations to describe the latter stages of transition is feasible.

It is interesting to examine the rate of approach to the asymptotic profile that is more conveniently done in terms of the average value of λ defined as follows:

$$\bar{\lambda} \equiv \frac{1}{4} \int_1^5 \lambda \, d\eta \tag{31}$$

Figure 4 shows $\bar{\lambda}$ as a function of displacement thickness Reynolds number Re_{δ^*}; note that $Re_{\delta^*_i}$ denotes the neutral-stability value of Re_{δ^*} for a given frequency. As shown, for the higher frequencies $\bar{\lambda}$ approaches its asymptotic value most rapidly. For $Fr = 0.5 \cdot 10^{-5}$, the lowest frequency at which computations have been done, the approach to the asymptotic values lie between $\bar{\lambda} = 0.066$ and $\bar{\lambda} = 0.083$, as compared to the postulated[11] turbulence-model value of 0.091.

Further examination of the $\bar{\lambda}$ variation with Reynolds number shows that, for the higher frequencies, the peak value is achieved at an amplification ratio of about e^4 while, for the

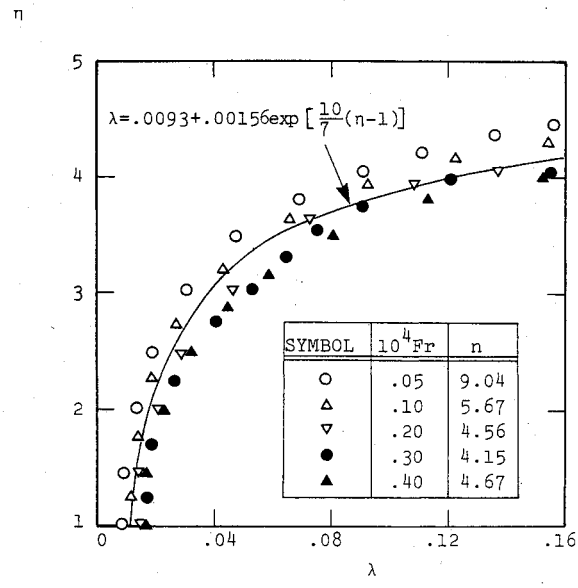

Fig. 3 Profiles of the closure coefficients λ for various frequencies and amplification ratios; zero pressure gradient.

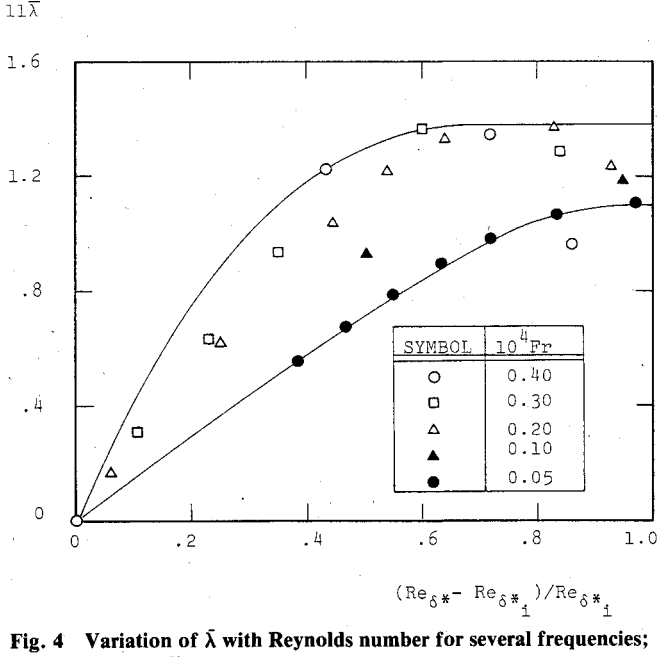

Fig. 4 Variation of λ̄ with Reynolds number for several frequencies; zero pressure gradient.

lowest frequency, $\bar{\lambda}$ is about half its asymptotic value at this ratio. Two key conclusions can be drawn from the computed variation of $\bar{\lambda}$. First, beyond an amplification ratio of e^4, $\bar{\lambda}$ varies slowly with Reynolds number. Second, $\bar{\lambda}$ is only weakly frequency dependent for frequencies in excess of $Fr = 10^{-5}$. These two points lend further credence to our hypothesis that turbulence-model equations potentially can yield a sound physical description of the latter stages of transition.

B. Initial Profiles

Having established Eq. (30) as a satisfactory correlation of computed $\bar{\lambda}$ profiles we now turn to initial profiles for e and ω that are needed to initiate a boundary-layer computation beyond the e^4-amplification point. Figures 5 and 6 show computed profiles for e and ω at the e^4-amplification point. These profiles have been obtained from the linear-stability computations and Eqs. (21) and (22). In each of the figures profiles are shown for five values of the dimensionless frequency Fr.

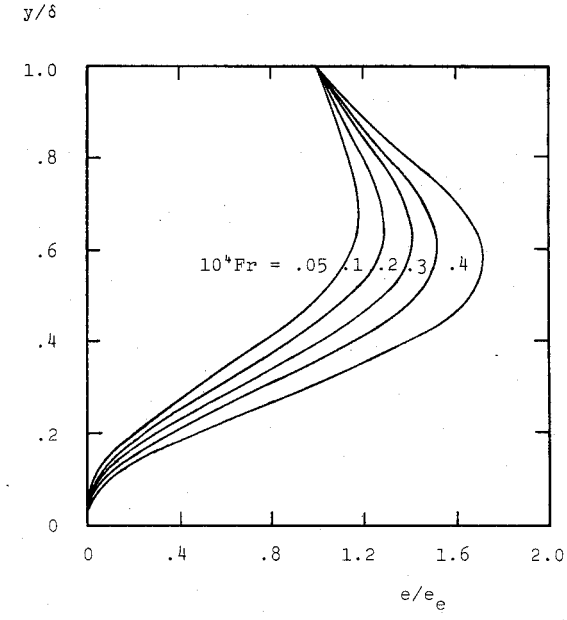

Fig. 5 Computed turbulent mixing-energy profiles after an initial disturbance has been amplified by a factor of e^4; zero pressure gradient.

The e profiles are displayed in terms of e/e_e vs y/δ where e_e is the value of e at the boundary-layer edge and δ is boundary-layer thickness. The ω profiles are parameterized as a function of Φ vs y/δ where Φ is defined by

$$\Phi = (\beta/20)\eta^2 (x\omega/U_e) \tag{32}$$

where the value of β is given in Eq. (7). As shown, the profiles are similar for the various frequencies although significant differences in amplitude are clearly indicated. These e and ω profiles have been fitted with cubic splines which yield a high degree of accuracy for values and slopes of the profiles.

C. Boundary Conditions

Before proceeding to the turbulence-model computations, boundary conditions must be specified at the boundary-layer edge, $y = \delta$. As in all previous computations, the boundary condition for e is determined by the freestream turbulence intensity according to

$$T' = 100\sqrt{\tfrac{2}{3}e_e}/U_e \tag{33}$$

where T' is turbulence intensity given in percent. To set the value of ω_e, we have analyzed the linear-stability predicted values. We have found empirically that at the e^4-amplification point, $\nu\omega_e/U_e^2$ correlates with the dimensionless frequency Fr according to the following empirical fit:

$$\nu\omega_{e_0}/U_e^2 = 28Fr^{7/4} \tag{34}$$

In Eq. (34), ω_{e_0} denotes the value of ω_e at the e^4-amplification point. Furthermore, according to the turbulence-model equation, ω_e satisfies Eq. (12) so that, in terms of the function Φ defined in Eq. (32), ω_e should vary with distance from the plate leading edge as

$$\frac{\omega_e}{\omega_{e_0}} = \left\{1 + \frac{5}{18}\Phi_e\left(\frac{x}{x_0} - 1\right)\right\}^{-1} \tag{35}$$

where Φ_e is the value of Φ at $y = \delta$ and x_0 is the value of x at the e^4-amplification point. Figure 7 compares the linear-stability computed variation of ω_e with the variation given by Eq. (35). As shown, the two variations are reasonably close. Hence, Eqs. (34) and (35) have been used in the computations.

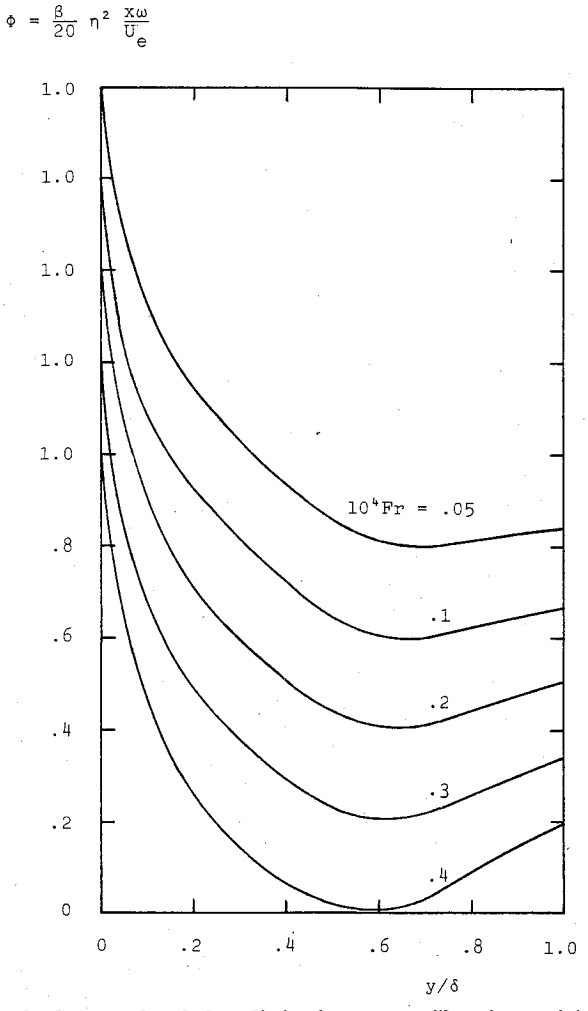

Fig. 6 Computed turbulent dissipation-rate profiles after an initial disturbance has been amplified by a factor of e^4; zero pressure gradient.

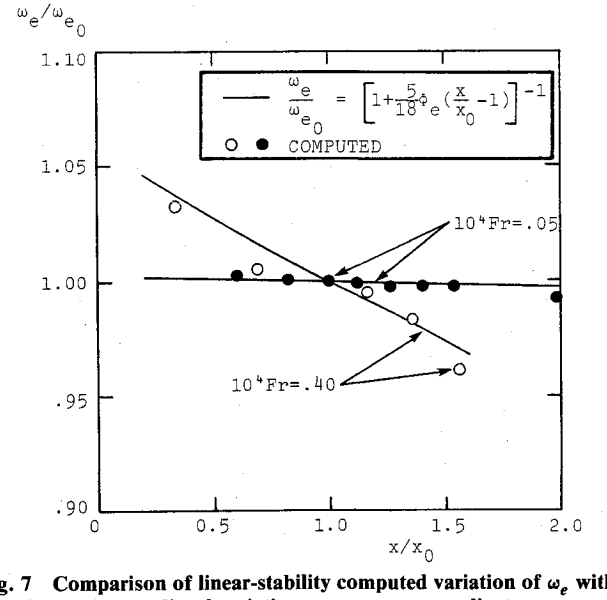

Fig. 7 Comparison of linear-stability computed variation of ω_e with model-equation predicted variation; zero pressure gradient.

Before proceeding to results of the computations, it is instructive to pause and discuss the implication of the derived boundary condition for ω. Unlike previous turbulence-model transition computations, we are not at liberty to arbitrarily specify ω_e. This is an important point because the boundary

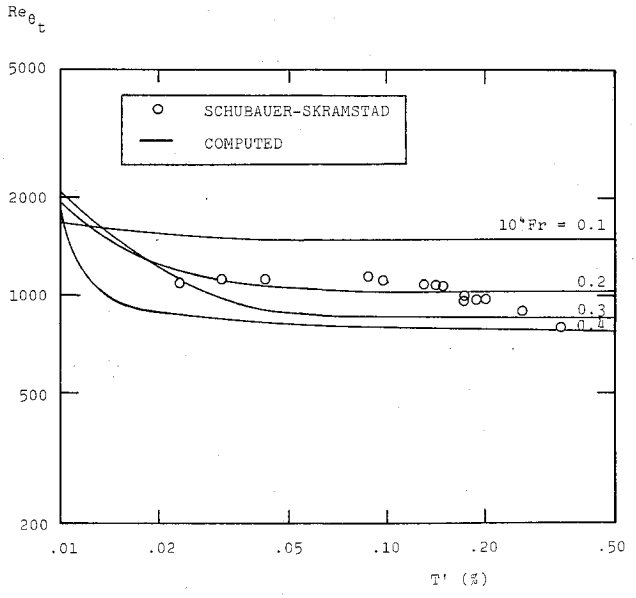

Fig. 8 Comparison of computed and measured transition momentum-thickness Reynolds number for the Blasius boundary layer.

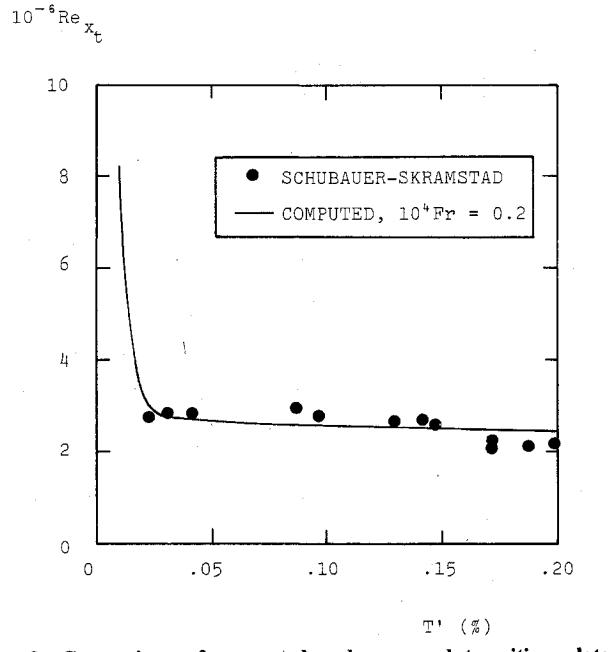

Fig. 9 Comparison of computed and measured transition plate-length Reynolds number for the Blasius boundary layer.

condition for ω has been ambiguous in the past and its specification has provided the equivalent of an "adjustable parameter" in the theory. Elimination of this adjustability enhances utility of the method, particularly if it proves to be an accurate predictive tool.

D. Transition Predictions

To assess the accuracy of the method, a series of computations has been performed for the Blasius boundary layer. In all calculations we have used: Eq. (30) to define λ, cubic spline fits for the initial e and ω profiles shown in Figs. 5 and 6, and Eqs. (33-35) to define boundary-layer edge conditions for e and ω. Further, in the computations, freestream turbulence intensity varies from 0.01 to 0.50% while $0.1 < 10^4 Fr < 0.4$. The upper bound on Fr has been chosen because $0.4 \cdot 10^{-4}$ is the highest frequency for which the stability diagram is sufficiently wide to permit amplification

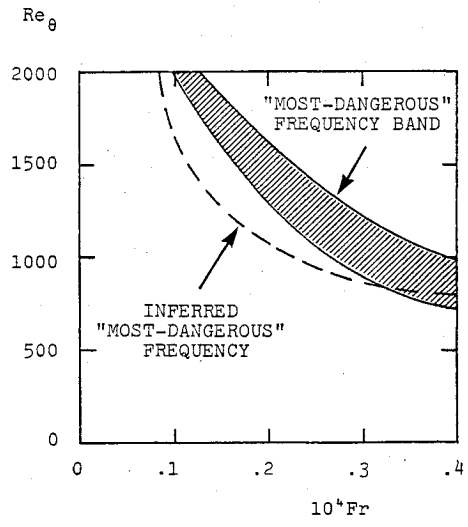

Fig. 10 Spectral effects.

much beyond a factor of e^4 so that our procedure becomes meaningless at higher frequencies. The lower bound on Fr has been chosen since the critical Reynolds number for $Fr = 10^{-5}$ is well above the transition Reynolds numbers observed by Schubauer and Skramstad,[14] indicating that lower frequencies are relevant only for much lower intensities than 0.01%. Since we are comparing our results with the Schubauer-Skramstad data that were taken for intensities in excess of 0.02%, this is a reasonable lower bound on Fr.

Figure 8 compares computed and measured transition momentum-thickness Reynolds number Re_{θ_t} for four frequencies, viz., $10^4\, Fr = 0.1$, 0.2, 0.3, and 0.4. This result is quite encouraging as this band of frequencies is comparable to that predicted by linear-stability theory[13] to be most unstable for the range of transition Reynolds numbers observed by Schubauer and Skramstad.

Figure 9 compares computed and measured transition Reynolds number based on distance from the plate leading edge Re_{x_t}; only the curve computed with $10^4\, Fr = 0.2$ is shown for simplicity. This figure displays an interesting feature of the computations, viz., that following the predicted variation of Re_{x_t} with T' down to about $T' = 0.03\%$ indicates an asymptote to a finite value of Re_{x_t} as $T' \to 0$, similar to the trend of the data. However below $T' = 0.03\%$, the predicted Re_{x_t} then increases rapidly implying that Re_{x_t} may approach an infinite value as $T' \to 0$. Although not shown in the figure, a similar trend appears for the other frequencies.

As evidence of the method's ability to properly treat spectral effects, Fig. 10 compares an inferred "most-dangerous" frequency with the linear-stability theory predicted most-dangerous frequency band. The inferred curve has been constructed by forcing agreement between model-predicted transition point and the Schubauer-Skramstad data. As shown, the curve lies just slightly outside the linear-stability theory band.

As a final note, the actual transition predictions have been found to be relatively insensitive to initial profiles. To make a similar claim about whether starting the turbulence-model computation at a different point (e.g., when the amplification ratio is e^3 or e^5) would require further research. Some computations have been done from the e^5-amplification point and this appeared to have little effect on the predicted transition point.

IV. Effects of Pressure Gradient

In order to investigate effects of pressure gradient, we now repeat the analysis of Sec. III using Falkner-Skan velocity profiles for both adverse and favorable pressure gradients. First, we compute λ profiles at the e^4-amplification point and seek a frequency-independent correlation. Then the boundary-layer edge condition for ω is correlated with frequency. Results follow.

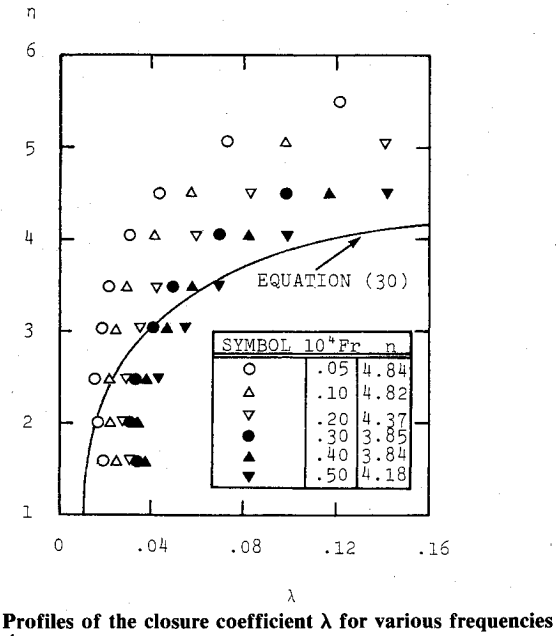

Fig. 11 Profiles of the closure coefficient λ for various frequencies near the e^4-amplification point; adverse pressure gradient.

A. Evaluation of the Closure Coefficient λ

The Falkner-Skan profiles satisfy the following equation:

$$\frac{d^3 f}{d\tilde{\eta}^3} + f\frac{d^2 f}{d\tilde{\eta}^2} + \beta_{FS}\left[1 - \left(\frac{df}{d\tilde{\eta}}\right)^2\right] = 0 \tag{36}$$

which is solved subject to

$$f = \frac{df}{d\tilde{\eta}} = 0 \text{ at } \tilde{\eta} = 0, = \frac{df}{d\tilde{\eta}} \to 1 \text{ as } \tilde{\eta} \to \infty \tag{37}$$

In Eq. (36), f is the dimensionless streamfunction so that the velocity u is obtained from

$$u = U_e \frac{df}{d\tilde{\eta}} \tag{38}$$

Also, the freestream velocity U_e is given by

$$U_e(x) = Cx^m \tag{39}$$

where C is a constant and m is related to the constant β_{FS} appearing in Eq. (36) through the following equation:

$$\beta_{FS} = 2m/(m+1) \tag{40}$$

Finally, the scaled coordinate $\tilde{\eta}$ is defined in terms of x, y, ν and U_e by

$$\tilde{\eta} = y\sqrt{\tfrac{1}{2}(m+1)(U_e/\nu x)} \tag{41}$$

Note that for zero pressure gradient $m = 0$ and Eq. (41) differs from Eq. (24) by a factor $\sqrt{2}$. For the sake of consistency with our earlier computations, all results in this section are cast in terms of η as defined in Eq. (24) rather than in terms of $\tilde{\eta}$.

For symmetry, we consider one adverse pressure gradient profile and one favorable pressure gradient profile, viz., we select

$$\beta_{FS} = -0.18, \quad \text{adverse} \quad \nabla p$$
$$\beta_{FS} = +0.18, \quad \text{favorable} \quad \nabla p \tag{42}$$

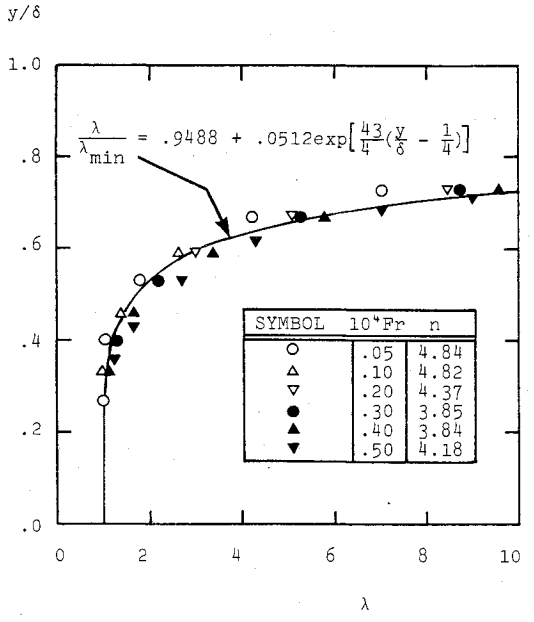

Fig. 12 Correlation of λ/λ_{min}; adverse pressure gradient.

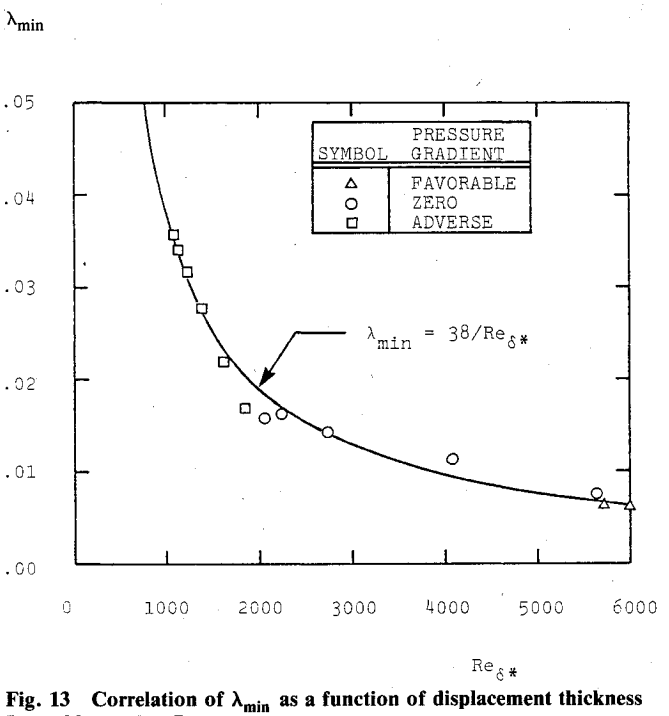

Fig. 13 Correlation of λ_{min} as a function of displacement thickness Reynolds number Re_{δ^*}.

which correspond to $m=-0.083$ and $m=+0.099$ for the adverse and favorable cases, respectively.

Turning first to adverse pressure gradient, Fig. 11 shows computed values of λ for several frequencies near the e^4-amplification point; the correlation for zero pressure gradient [Eq. (30)] is shown for reference. As can be seen, the various λ profiles show a stronger frequency dependence than exists in the absence of pressure gradient. Furthermore, the disparity in the various profiles fails to diminish as η increases. Close examination of the computed results shows that the minimum value of λ increases as Fr increases. This trend is also present for zero pressure gradient (see Fig. 3), although not as pronounced as for $\beta_{FS}=-0.18$. This observation suggests that a better correlation might be obtained by working with the ratio of λ to its minimum value, λ_{min}. Figure 12 shows that the ratio λ/λ_{min} does indeed correlate nicely; the correlation is

$$\frac{\lambda}{\lambda_{min}}=0.9488+0.0512\exp\left\{\frac{43}{4}\left(\frac{y}{\delta}-\frac{1}{4}\right)\right\};\ \beta_{FS}=-0.18 \quad (43)$$

Re-examination of the zero pressure-gradient data shows that rewriting Eq. (30) in terms of λ/λ_{min} and y/δ improves the correlation; the revised correlation is

$$\frac{\lambda}{\lambda_{min}}=0.8564+0.1436\exp\left\{\frac{60}{7}\left(\frac{y}{\delta}-\frac{1}{6}\right)\right\};\ \beta_{FS}=0 \quad (44)$$

Turning finally to favorable pressure gradient, we find similar results to those obtained with zero and adverse gradients, i.e., λ/λ_{min} is weakly frequency dependent. The favorable gradient correlation is

$$\frac{\lambda}{\lambda_{min}}=0.604+0.396\exp\left\{\frac{48}{7}\left(\frac{y}{\delta}-\frac{1}{6}\right)\right\};\ \beta_{FS}=+0.18 \quad (45)$$

As a final comment, examination of the computed values of λ_{min} shows that an excellent correlation of λ_{min} can be devised which is independent of pressure gradient. Specifically, λ_{min} is found to vary inversely with displacement-thickness Reynolds number Re_{δ^*}, according to the following formula:

$$\lambda_{min}=38/Re_{\delta^*} \quad (46)$$

Figure 13 compares computed values of λ_{min} with Eq. (46).

B. Boundary Conditions

As the initial profiles appear to have little effect on transition predictions attending use of the established procedure, we now proceed directly to boundary conditions. Again we use Eq. (33) to define the boundary-layer edge value of the turbulent mixing energy. Also, Eq. (35) remains valid for determining ω_e/ω_{e_0} although the validity of Eq. (34) must be ascertained.

As in the $\beta_{FS}=0$ case, we find that $\nu\omega_{e_0}/U_e^2$ is proportional to $Fr^{7/4}$ for adverse and favorable gradient also. Furthermore, Eq. (34) correlates all of the data to within a few percent. Hence, even in the presence of pressure gradient, the edge value of ω is uniquely determined as a function of the frequency of the disturbance.

V. Discussion

While some fine tuning of the procedure is needed, the results described in Secs. III and IV are very encouraging. Our proposed synthesis of the linear-stability and turbulence-model transition-prediction methods appears to be quite sensible. On the one hand, using linear-stability theory in the initial stages of the transition phenomenon (i.e., up to the e^4-amplification point) provides a physically-sound procedure which takes proper account of spectral effects. On the other hand, we believe that using the turbulence-model equations to describe the latter stages of transition with starting profiles for e,ω, and λ and the boundary-layer edge boundary condition on ω as predicted by linear-stability theory is more physically sound than continuing beyond the e^4-amplification point with linear-stability theory.

We wish to emphasize the importance of knowing the proper value of ω_e. As noted earlier, uncertainty about the value of ω_e has left the turbulence-model transition-prediction method with an effective "adjustable parameter" in previous analyses. Removing this uncertainty is an important conceptual advance. It is also important to note that the value of ω_e is frequency dependent so that, as would be expected on physical grounds, the latter stages of transition are predicted to be not entirely independent of spectral effects. While we have yet to find a physical explanation for the proportionality of ω_e and $Fr^{7/4}$, we continue to seek such an explanation.

In conclusion, results to date show great promise for development of a physically-sound alternative to the e^9 procedure. Further research should be conducted to determine how well the method predicts transition-point location for well-documented flows with adverse and/or favorable pressure gradient. Also, further testing is needed to establish more definitively the method's sensitivity to the point of initiation of the turbulence-model phase of the computation. When such analyses have been done we feel confident a reliable analytical tool for predicting boundary-layer transition will result.

Acknowledgment

Research was sponsored by the Office of Naval Research under Contracts N00014-77-C-0259 and N00014-78-C-0799.

References

[1] Wazzan, A. R. and Smith, A.M.O., "Laminarization of Water Boundary Layers over Bodies of Revolution," Paper presented at RAND Low-Speed Boundary-Layer Transition Workshop, The RAND Corp., Santa Monica, Calif., Sept. 1976.

[2] Smith, A.M.O. and Gamberoni, N., "Transition, Pressure Gradient, and Stability Theory," Douglas Aircraft Co., Inc., El Segundo, Calif., Rept. ES 26388, 1956.

[3] van Ingen, J. L., "A Suggested Semiempirical Method for the Calculation of the Boundary Layer Transition Region," Dept. Aero. Eng., Institute of Technology, Delft, Rept. V.T.H. 74, 1956.

[4] Wilcox, D. C., "Turbulence-Model Transition Predictions," *AIAA Journal*, Vol. 13, Feb. 1975, pp. 241-243.

[5] Jones, W. P. and Launder, B. E., "Calculation of Low Reynolds Number Phenomena with a Two-Equation Model of Turbulence," *International Journal of Heat and Mass Transfer*, Vol. 16, 1973, pp. 1119-1129.

[6] Donaldson, C. duP., "A Computer Study of an Analytical Model of Boundary Layer Transition," AIAA Paper 68-38, New York, N.Y., Jan. 1968.

[7] Wilcox, D. C. and Chambers, T. L., "Numerical Simulation of Nosetip Transition: Model Refinement and Validation," AFOSR-TR-76-1112, 1976.

[8] Chambers, T. L. and Wilcox, D. C., "Application of the Turbulence-Model Transition-Prediction Method to Flight-Test Vehicles," *Turbulence in Internal Flows*, edited by S. B. Murthy, Hemisphere Publishing Co., 1976, pp. 233-247.

[9] Wilcox, D. C. and Chambers, T. L., "Transition Simulation for Incompressible Boundary Layers and Heated Hydrodynamic Bodies," DCW Industries, Inc., Studio City, Calif., Rept. DCW-R-10-01, 1976.

[10] Wilcox, D. C. and Traci, R. M., "A Complete Model of Turbulence," AIAA Paper 76-351, San Diego, Calif., July 1976.

[11] Wilcox, D. C., "A Model for Transitional Flows," AIAA Paper 77-126, Los Angeles, Calif., Jan. 1977.

[12] Wilcox, D. C. and Chambers, T. L., "Streamline Curvature Effects on Turbulent Boundary Layers," *AIAA Journal*, Vol. 15, April 1977, pp. 574-580.

[13] Mack, L. M., "Transition and Laminar Instability," Jet Propulsion Laboratory, Pasadena, Calif., Pub. 77-15, 1977.

[14] Schubauer, G. B. and Skramstad, H. K., "Laminar Boundary-Layer Oscillations and Transition on a Flat Plate," NACA 909, 1948.

From the AIAA Progress in Astronautics and Aeronautics Series..

EXPERIMENTAL DIAGNOSTICS IN COMBUSTION OF SOLIDS—v. 63

Edited by Thomas L. Boggs, Naval Weapons Center, and Ben T. Zinn, Georgia Institute of Technology

The present volume was prepared as a sequel to Volume 53, *Experimental Diagnostics in Gas Phase Combustion Systems*, published in 1977. Its objective is similar to that of the gas phase combustion volume, namely, to assemble in one place a set of advanced expository treatments of the newest diagnostic methods that have emerged in recent years in experemental combustion research in heterogenous systems and to analyze both the potentials and the shortcomings in ways that would suggest directions for future development. The emphasis in the first volume was on homogenous gas phase systems, usually the subject of idealized laboratory researches; the emphasis in the present volume is on heterogenous two- or more-phase systems typical of those encountered in practical combustors.

As remarked in the 1977 volume, the particular diagnostic methods selected for presentation were largely undeveloped a decade ago. However, these more powerful methods now make possible a deeper and much more detailed understanding of the complex processes in combustion than we had thought feasible at that time.

Like the previous one, this volume was planned as a means to disseminate the techniques hitherto known only to specialists to the much broader community of reesearch scientists and development engineers in the combustion field. We believe that the articles and the selected references to the current literature contained in the articles will prove useful and stimulating.

339 pp., 6 × 9 illus., including one four-color plate, $20.00 Mem., $35.00 List

TO ORDER WRITE: Publications Dept., AIAA, 1290 Avenue of the Americas, New York, N.Y. 10019